BMC Gastroenterology

RESEARCH

Open Access

# Emodin protects against severe acute pancreatitis-associated acute lung injury by activating Nrf2/HO-1/GPX4 signal and inhibiting ferroptosis in vivo and in vitro

Gang Shen[1,5†], Haiyun Wen[1,2,3†], Huijuan Li[3,4], Xuetao Zhang[1,2,3], Bowen Lan[1,3], Xuanchi Dong[1,3], Peng Ge[1,2,3], Yalan Luo[6] and Hailong Chen[1,2,3*]

## Abstract

**Background** Severe acute pancreatitis (SAP) has high morbidity, a complicated and dangerous course, and many complications, including severe pulmonary complications. SAP-associated acute lung injury (SAP-ALI) is still a significant challenge for surgeons because of its high mortality. Therefore, more effective treatment methods are urgently needed. Emodin (EMO) has shown tremendous potential in treating many refractory diseases. However, its protection mechanism in SAP-ALI needs to be further clarified. This study was undertaken to investigate the protective effects of EMO against lung injury in SAP rats and alveolar epithelial cells, with a particular focus on the classical ferroptosis pathway.

**Methods** In an in vivo study, forty SD rats were evenly split into five groups: sham operation (SO) group, the biliopancreatic duct was retrogradely injected with 5% sodium taurocholate (STC) to create the SAP group, SAP + EMO group was administered EMO via gavage to the rats following the modeling, SAP + ML385 group (a given inhibitor of nuclear factor erythroid 2-related factor 2 (Nrf2)), SAP + ML385 + EMO group. In an in vitro study, alveolar epithelial A549 cell lines were exposed to lipopolysaccharide (LPS) and treated with EMO. ML385 was also used to inhibit the expression of Nrf2. Pancreatic and lung tissue damage was evaluated using histological examination and molecular experiments. Enzyme-linked immunosorbent assays (ELISA) were used to assess the levels of pro-inflammatory cytokines, $Fe^{2+}$, and associated oxidative stress indicators in the serum and cell supernatant. Real-time polymerase chain reaction (PCR), Western blot (WB), and immunofluorescence were used to find the expressions of related mRNAs and proteins in the lung tissue or A549 cells.

**Results** The findings demonstrated that suppressing Nrf2 expression exacerbated the inflammatory response brought on by SAP and the pathological alterations of SAP-ALI. Emodin treatment reversed this pathological change by activating the Nrf2/Heme Oxygenase-1 (HO-1)/glutathione peroxidase 4 (GPX4) signal path. Moreover,

†Gang Shen and Haiyun Wen contributed equally to this work.

*Correspondence:
Hailong Chen
chenhailong@dmu.edu.cn

Full list of author information is available at the end of the article

these results also showed that EMO, contrary to the effects of ML385, suppressed the ferroptosis response, which manifested as up-regulated glutathione (GSH) and GPX4 levels in vivo and in vitro and down-regulated malondialdehyde (MDA), superoxide dismutase (SOD), $Fe^{2+}$, and reactive oxygen species (ROS) levels.

**Conclusions** Our results demonstrated that EMO effectively inhibited ferroptosis both in vivo and in vitro, while also modulating the Nrf2/HO-1/GPX4 signaling pathway to provide protection against SAP-ALI.

**Keywords** Ferroptosis, SAP-ALI, Emodin, Nrf2, GPX4, HO-1

## Background

Severe acute pancreatitis (SAP) mainly refers to a variety of factors, the patient's pancreatic enzymes are abnormally activated, there is pancreatic tissue edema, and in severe cases, it will cause various inflammatory reactions, pancreatic necrosis, or hemorrhage. It is a disease commonly found in gastroenterology [1, 2]. Damage to capillary endothelial cells and alveolar epithelial cells results from SAP complicated by acute lung injury (ALI), which can manifest as respiratory failure with progressive, acute, and hypoxic characteristics. The main pathological changes are decreased lung volume and lung compliance and a serious imbalance of ventilation and blood flow [3]. Therefore, it is of great scientific significance and clinical application value to study the pathogenesis of SAP-ALI and seek efficient therapeutic drugs and methods.

A novel form of programmed cell death known as ferroptosis is typified by oxidative damage and intracellular iron overload. Ferroptosis is a significant factor in several illnesses, including retinal excitotoxic lesions, neuropathy, pulmonary fibrosis, etc [4–6]. According to current reports, acute pancreatitis-related renal injury is influenced by ferroptosis [7]. There is also research indicating the importance of ferroptosis in ALI. In recent years, through animal and cell model experiments, ferroptosis was closely related to ALI brought on by sepsis and intestinal ischemia/reperfusion [8–10].

It is discovered that the antioxidant response element (ARE) mediates gene expression and nuclear factor erythroid 2-related factor 2 (Nrf2) is a key regulatory factor in this process [11]. The endogenous protective substance heme oxygenase-1 (HO-1) guards against oxidative damage [12]. One marker protein for ferroptosis is glutathione peroxidase 4 (GPX4) [13]. The Nrf2/HO-1/GPX4 signaling pathway functions as a protective chain for multiple organs in varying stress conditions, and it is of significant value to study the signal axis for targeted therapy of SAP-ALI.

Emodin (EMO) is a natural compound extracted from rhubarb with many therapeutic effects, such as antioxidant, antibacterial, immune regulation, and anti-inflammatory [14, 15]. The protective effect of EMO against lung injury has been thoroughly studied by academics both domestically and overseas. EMO can improve lung injury in the following ways: inhibiting activation and pyroptosis of alveolar macrophages [16, 17], modulating exosome-specific miRNA expression profiles [18], and regulating apoptosis [19]. It is yet unknown how ferroptosis mediated by EMO functions in the pathophysiology of SAP-ALI. Therefore, this paper intends to analyze how EMO regulates ferroptosis by targeting the Nrf2/HO-1/GPX4 signaling pathway in vivo and in vitro, reducing lung injury and inhibiting disease development in SAP rats.

## Methods

### Animals and experimental design

Beijing Sibeifu Biology Technology Co., Ltd. provided forty male SPF-grade SD rats, weighing 180 ± 20 g and aged 6 to 8 weeks. The animal production license was SCXK (Jing) -2019-0010. The rats lived in a 20 ± 2 °C environment with 60–70% relative humidity and a 12-hour light/dark cycle. They were given access to food and water without restriction. All procedures involving animals in this study had prior approval from Dalian Medical University's Laboratory Animal Ethics Committee (animal ethics approval number: AEE23067). As mandated by China Animal Protection and Use Committee regulations, every effort was made to guarantee the comfort and welfare of the animals throughout the studies.

Forty SD rats were randomly assigned into five groups: the SO group, SAP group, SAP + EMO group, SAP + Nrf2 inhibitor group (SAP + ML385 group), and SAP + ML385 + EMO group (Fig. 1A). Before modeling, every rat was fed regularly and housed in the same conditions for one week. Thirty minutes before surgery, rats in the SAP + ML385 and SAP + ML385 + EMO groups received an intraperitoneal injection of 30 mg/kg of the Nrf2 inhibitor ML385. Rats were undergoing laparotomy in the SO group. They received a retrograde injection of normal saline into the common bile duct, whereas other groups received an injection of 5% sodium taurocholate into the same bile duct to cause SAP. Emodin (40 mg/kg) was given to the EMO group and SAP + ML385 + EMO group at 2 h and 12 h postoperatively. 24 h after modeling, all rats were anesthetized by intraperitoneal injection of 1% pentobarbital sodium (4 mg/100 g). Serum was collected from euthanized rats 24 h after modeling and pancreatic tissue and lung tissue were extracted for molecular experiments.

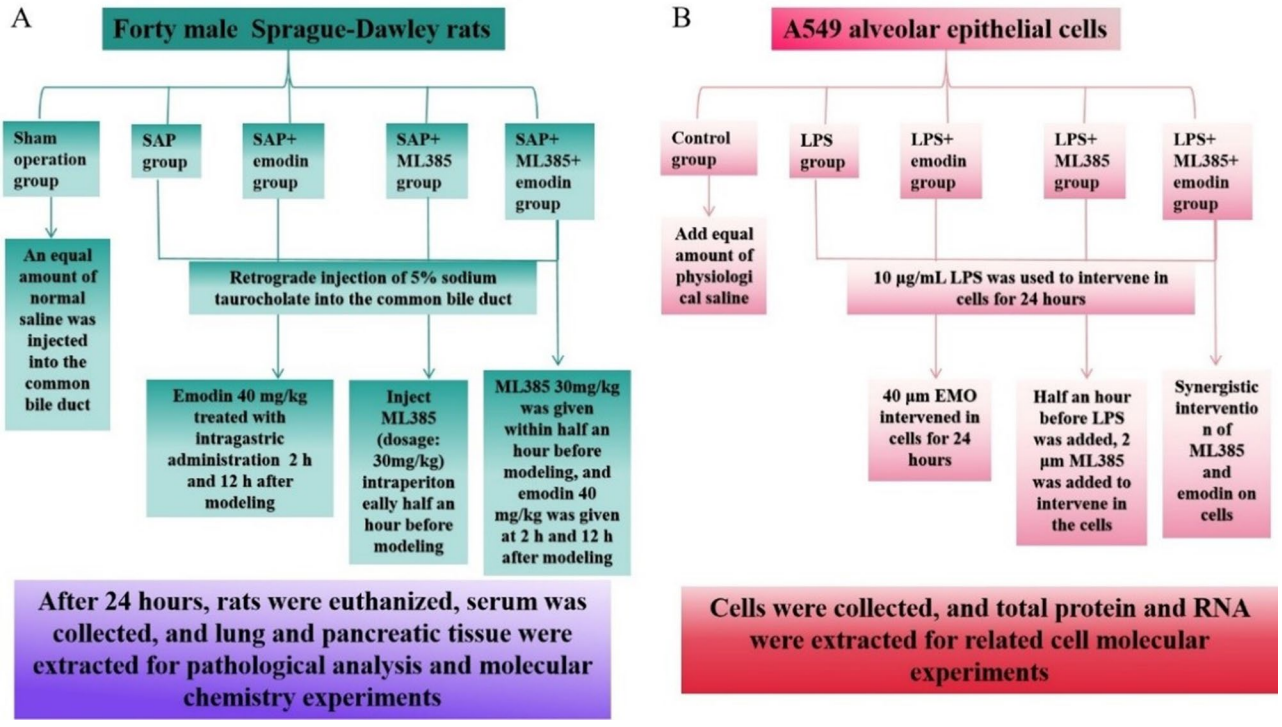


**Fig. 1** Experimental design schematic diagram. (**A**) In vivo study design. (**B**) In vitro study design

### Cells and experimental design

The BeNa Culture Collection (BNCC) provided the alveolar epithelial cell line A549. They were inoculated in Ham's F-12 K medium containing 1% penicillin-streptomycin and 10% FBS and cultivated in a 5% CO2 incubator at 37 ℃. Cells were passaged every two to three days (the cell density needed to reach 80% for passage) and their culture medium changed every one to two days, depending on their growth conditions. Logarithmic cells were taken for experimental determination.

Five cell groups were designed: control (CON), LPS, LPS + EMO, LPS + ML385, and LPS + ML385 + EMO (Fig. 1B). Administered concentrations were 10 μg/mL for LPS, 40 μM for EMO, and 2 μM for ML385. Thirty minutes before adding LPS, ML385 was added. Following 24 h of LPS action, EMO was added.

### Chemicals and reagents

Thermo Fisher Scientific Inc. (USA) provided the sodium taurocholate. ML385 was supplied by ApexBio Technology (USA). IL-1β (Cat# F15810) and TNF-α (Cat# F16960) were obtained from WESTANG BIO-TECH CO., LTD (Shanghai, China). We bought the following products from Elabscience (Wuhan, China): Amylase Activity Assay Kit (Cat# E-BC-K006-M), Ferrous Iron Colorimetric Assay Kit (Cat# E-BC-K773-M), SOD (Cat# E-BC-K020-M), GSH (Cat# E-BC-K030-M), MDA (Cat# E-BC-K025-M), and IL-18 (Cat# E-EL-R0567c). The PTGS2 ELISA Kit (Cat# CB14167-Ra) was purchased from COIBO (Shanghai, China). RIPA buffer was purchased from JRDUN Biotech (Shanghai, China). Emodin, KeyGEN Bio TECH BCA protein quantification kit, and SDS-PAGE gels were purchased from Solarbio (Beijing, China). RNAex Pro reagents (Cat# AG21102), Evo M-MLV Reverse Transcription Premix Kit (Cat# AG11728), and SYBR Green Premix Pro Taq HS qPCR Kit II (Cat# AG11702) were obtained from Accurate Biology (Hunan, China). Electron microscope fixative (Cat# J1102), PBS buffer (Cat# G0002), DAPI staining reagent (Cat# G1012), and anti-fluorescence quenching sealing tablets (Cat# G1401) were obtained from Jijia Biotechnology Co., Ltd. (Liaoning, China). 812 embedding agent (Cat# 90529-77-4) was purchased from SPI. Anhydrous ethanol and acetone were obtained from Sinopharm Chemical Reagents Co., Ltd. (Shanghai, China). ROS dye liquor was purchased from Sigma Aldrich (Shanghai, China).

### Histological analysis

The fully fixed rat pancreas, or lung tissue, was taken out of 4% paraformaldehyde and cut into pieces. HE staining was performed according to the steps of dehydration, transparency, embedding, slicing, dewaxing, dyeing, dehydration, and sealing, and images were observed and collected under the microscope. Pancreatic edema, inflammation, acinar necrosis, and hemorrhage were evaluated on a scale from 0 to 4 [20]; pulmonary edema, hemorrhage, and leukocyte infiltration were each scored

from 0 to 3 [21]. Each group was randomly selected for three sections, and three different fields of view were observed for each section.

#### Measurement of Wet/Dry ratio of lung tissue

After removing lung tissue from each group of rats, the wet weight was promptly measured. After drying in an oven at 65 °C for 72 h, the lung tissue was weighed again and recorded as dry weight.

#### Enzyme-linked immunosorbent assay

ELISA kit was used to analyze the contents of amylase and serum or cell supernatant inflammatory factors, namely IL-1β, TNF-α, and IL-18. Ferroptosis markers $Fe^{2+}$ and PTGS2, as well as oxidative stress indicators MDA, SOD, and GSH in rat lung tissue were examined with 10% lung tissue homogenate. PTGS2, SOD, and GSH levels in cells were measured using particular kits.

#### Transmission electron microscope assay

Fresh rat lung tissues taken from each group, the volume of which is generally less than 1 mm×1 mm×1 mm, were quickly put into a 4 °C electron microscope-fixed solution for 2 ~ 4 h. After washing with 0.1 M phosphate buffer PB (PH7.4), it was fixed with 11% osmic acid·0.1 M phosphate buffer PB (PH7.4) at 20 °C. Following this were dehydration, infiltration, and embedding operations. Cut skinny slices, 60–80 nm. Subsequently, the slices were left to dry overnight at room temperature using uranium and lead double staining. Finally, use a transmission electron microscope to observe and gather images for analysis.

#### Molecular docking

Numerous studies have demonstrated the effectiveness of EMO in treating SAP [18, 22]. To verify the correlation between EMO and the target proteins of the classical pathway of ferroptosis induced by SAP. We simulated the molecular docking between EMO and Nrf2, HO-1, and GPX4 in the AutoDockTools-1.5.7 software. First, the crystal structures of Nrf2, HO-1, and GPX4 were downloaded from the PDB database (https://www.rcsb.org), and the 3D structure of emodin was obtained from the PubChem database (https://pubchem.ncbi.nlm.nih.gov). Use PyMol 2.5.5 software to remove water molecules and organic compounds from the receptor protein. Then, the target protein, after removing water molecules and emodin, is introduced into AutoDockTools-1.5.7 for structural optimization and treatment and then docked. A lower binding energy of the ligand-target protein complex is linked to improved binding activity. Ultimately, the results are visualized using PyMol software.

**Table 1** Antibodies for Western blot

| Antibody | Dilution | Species | Supplier | Catalogue number |
|---|---|---|---|---|
| Nrf2 | 1:1000 | Rabbit | Affinity | AF0639 |
| HO-1 | 1:1000 | Rabbit | Affinity | AF5393 |
| GPX4 | 1:1000 | Rabbit | Abclonal | A11243 |
| β-actin | 1:50000 | Rabbit | Abclonal | AC026 |

#### Cell viability assay

Take A549 cells in the logarithmic growth period, inoculate 100 μL cell suspension (cell density is $5 \times 10^3$/mL) into a 96-well plate, and after cell adherent growth for 24 h, add culture solution containing emodin or ML385 with different concentration gradients for culture, with 6 holes in each group and another blank group. Put 10 μL of CCK-8 working solution into each well after the 24 and 48-hour culture period, and then incubate for one hour. An enzyme-labeled device (BioTek, America) was used to measure the absorbance (A) of each well at a wavelength of 450 nm, and the cell viability was computed. IC50 is calculated by a 4-parameter regression of the logarithmic transformation curve using GraphPad Prism.

#### Western blot

Lungs from each group of rats were collected. Protein extraction and quantification were performed using RIPA buffer and the BCA protein quantification kit. After protein concentration quantification, each set of lysate samples (10 μl/lane) was separated on 8-12% SDS–PAGE gels and transferred to polyvinylidene difluoride membranes. TBST containing 5% skim milk was used to block the membranes for an hour. Primary antibodies against Nrf2, HO-1, GPX4, and β-actin were incubated on the membranes for an entire night at 4 °C. The secondary antibody was incubated for 2 h at room temperature the next day. The images were taken with a Tanon 5200 imaging system and developed using an upgraded chemiluminescence reagent (Keygen). Next, the optical density analysis feature of ImageJ 1.8.0 software was utilized to count the relative amounts of β-actin and the target protein. Table 1 displays details about antibodies.

#### PCR analysis

Following total RNA isolation from lung tissue and alveolar epithelial cells using RNAex Pro reagents. RNA samples were reverse transcribed into cDNA using the Evo M-MLV Reverse Transcription Premix Kit. Using a SYBR Green Premix Pro Taq HS qPCR Kit II and particular primer sequences (Table 2), gene amplification was carried out in a LineGene 9600 Plus real-time PCR machine. PCR conditions were initial denaturation at 95 °C for 30 s, denaturation at 95 °C for 5 s for 40 cycles, cooling, and extension at 64 °C for 30 s. Finally, the $2^{-\Delta\Delta CT}$ approach was used to analyze data from gene mRNA transcripts. Three independent experiments were conducted for each group.

**Table 2** The sequences of primers

| Geng | Species | Forward primer (5′→3′) | Reverse primer (5′→3′) |
|---|---|---|---|
| Nrf2 | Rat | ATTGCCACCGCCAGGACTA | GGAGTTGCTCTT-GTCTCTCCTT |
| HO-1 | | ACAGACAGAGTTTCTTC-GCCAGA | ATAAATTCCCACT-GCCACGGTC |
| GPX4 | | CCGCTGTGGAAGTGGAT-GAAGATC | CTTGTCGATGAG-GAACTGTGGAG |
| GAPDH | | GGCACAGTCAAGGCT-GAGAATG | ATGGTGGT-GAAGACGCCAGTA |
| Nrf2 | Human | TCCATTCCTGAGTTACAGT-GTCTT | GGCTTCTG-GACTTGGAACCAT |
| HO-1 | | CTGCGTTCCTGCTCAACATC | GCTCTGGTCCTTG-GTGTCAT |
| GPX4 | | CAGTGAGGCAAGACC-GAAGTA | CGAACTGGTTA-CACGGGAAGG |
| GAPDH | | GCACCGTCAAGGCT-GAGAAC | TGGTGAAGACGC-CAGTGGA |

#### Immunofluorescence assay

After the cells were cultured for a proper time, they were climbed onto the cover glass. After the cell culture adhered to the wall, the medium was sucked out, washed twice with PBS, fixed for 30 min with 2 ml of paraformaldehyde, and then sucked out. To prevent the loss of antibodies, after shaking the slide slightly, draw a circle in the center of the cover glass with a histochemical pen. Add 50–100 μl of the membrane-breaking working solution, let it sit at 25 ℃ for 20 min, and then wash it with PBS. After that, the tissue was uniformly covered with 3% BSA by dripping it into the circle, and it was sealed and left to stand at 25 ℃ for 30 min. Shake off the sealing solution gently, then pour a specific amount of the Nrf2 antibody made with PBS into the cell orifice plate. Keep the plate flat in a wet box at 4 °C overnight. Incubate for 50 min at room temperature after adding the matching secondary antibody the following day. The nucleus was then re-stained with DAPI, and the slide was sealed with anti-fluorescence-quenching tablets. Finally, the image is collected.

#### ROS fluorescence probe detection

The cell treatment slides resembled the 4.12 immunofluorescence first step. Subsequently, the ROS dye solution was poured into the circle and allowed to sit at 37 °C in a lightproof incubator for 30 min. DAPI stained the nucleus again, and the anti-fluorescence quenching tablets were sealed. Ultimately, the picture is gathered.

#### Statistical analysis

In this study, data (from a minimum of three independent experiments conducted in each group) are represented as mean ± standard error or as representative images. The means of the groups were compared using a one-way analysis of variance (ANOVA). The programs utilized for statistical analysis and visualization were SPSS 24.0 and GraphPad Prism 10.0. A p-value of less than 0.05 is considered statistically significant.

## Results

#### EMO treatment can alleviate the inflammatory reaction of SAP rats by activating Nrf2

The pancreatic tissue was examined for pathology (Fig. 2A). The SO group rats exhibited normal pancreas morphology, while the SAP rats displayed significant edema, necrosis, and inflammatory cell infiltration, and the overall histological score increased significantly (Fig. 2B). Compared to the SAP group, the pathological damage to the pancreatic tissue in the SAP + ML385 group was more evident, but the EMO treatment mitigated all of the pathological alterations. In addition, rats in the SO group had substantially lower serum amylase activity than rats in the SAP group, and rats in the SAP + ML385 group had higher serum amylase activity than rats in the SAP group (Fig. 2C). However, EMO may inhibit serum amylase activity by activating Nrf2. The SAP or SAP + ML385 group had higher levels of IL-1β, TNF-α, and IL-18 than the SO group, and the expression levels of these inflammatory factors decreased significantly after EMO treatment (Fig. 2D-F). Consequently, inhibition of Nrf2 expression aggravated the inflammatory reaction induced by SAP in rats, and emodin treatment reversed this pathological change by activating Nrf2.

#### Effect of EMO or Nrf2 inhibitor on lung injury induced by SAP

The results of HE staining indicated that the SAP group had more severe pulmonary edema than the SO group, more severe alveoli, increased wall thickening, and increased infiltration of inflammatory cells, particularly in the Nrf2 inhibitor group. These histopathological alterations were considerably reduced following EMO treatment (Fig. 3A). Compared with the SAP group, the lung histological score of EMO-treated rats was decreased dramatically (Fig. 3B), the ratio of wet/dry (W/D) weight of lung tissue was significantly reduced (Fig. 3C), and the degree of edema was effectively improved. These results show that EMO alleviates the lung injury induced by SAP in the histological layer, and may work by activating Nrf2.

#### Effects of EMO on oxidative damage and ferroptosis in SAP-ALI rats

The level of $Fe^{2+}$ was measured, and it was found that ML385 could increase the accumulation of $Fe^{2+}$ in the lung tissue (Fig. 4A). In addition, ML385 markedly elevated the levels of prostaglandin-endoperoxide synthase 2 (PTGS2) and malondialdehyde (MDA) in the lung tissue of SAP rats (Fig. 4B, D). However, the contents of

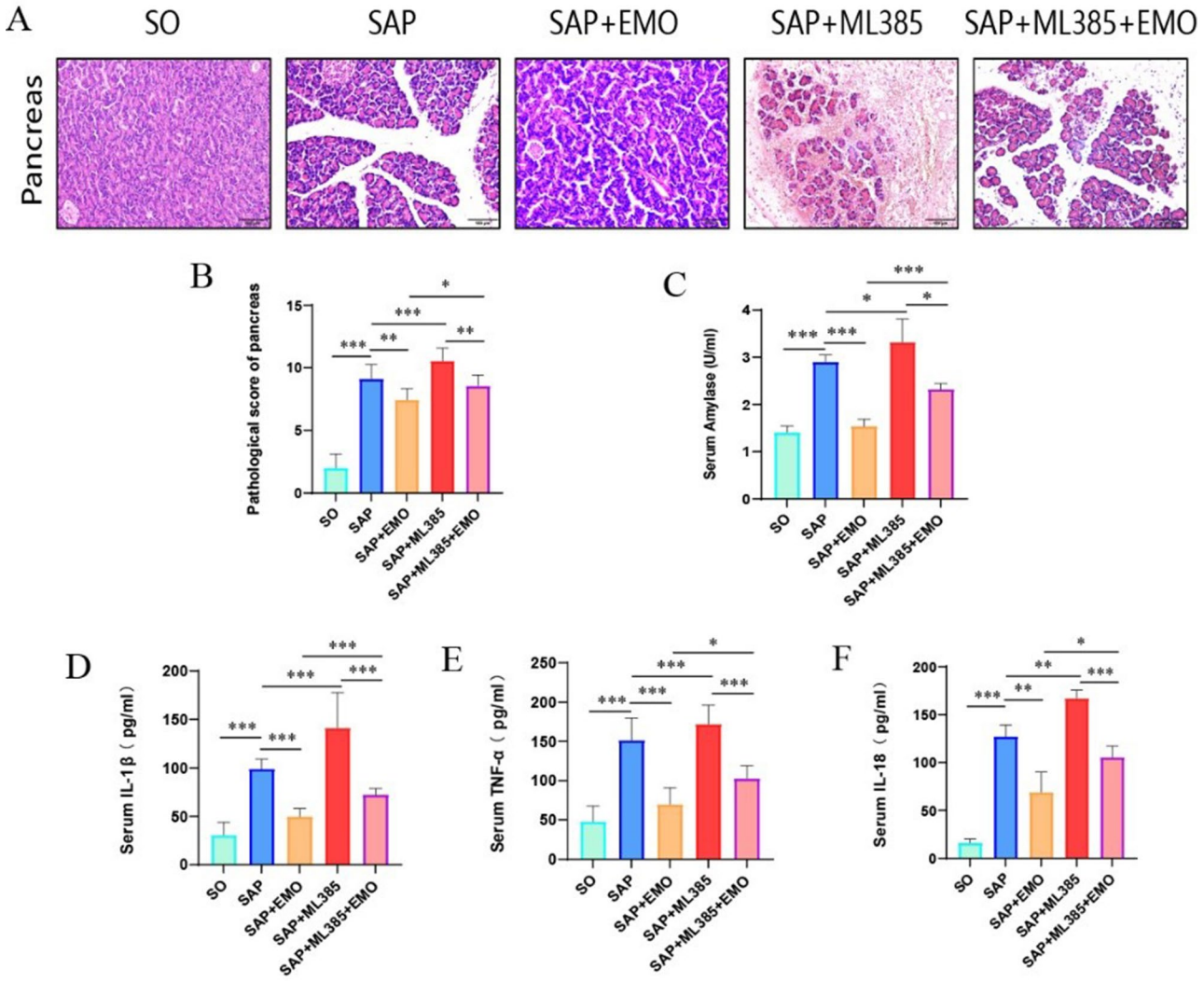


**Fig. 2** EMO treatment can alleviate the inflammatory reaction of SAP rats caused by Nrf2 down-regulation by activating Nrf2. (**A**) Pancreatic tissue stained with hematoxylin-eosin (HE) (scale bar, 100 μm). (**B**) Quantitative analysis of pathological scores. (**C**) Analysis of serum amylase activity. (**D** - **F**) Analysis of serum levels of IL-1β, TNF-α, and IL-18. ***$p < 0.001$, **$p < 0.01$, *$p < 0.05$

glutathione (GSH) and superoxide dismutase (SOD) in rats treated with ML385 decreased (Fig. 4C, E). Interestingly, changes in oxidative damage and ferroptosis-related indexes after EMO administration were significantly reversed (Fig. 4A-E). Figure 4F showed that under the transmission electron microscope (TEM), the SO group was found to have normal mitochondria with clearly visible mitochondrial cristae. In the SAP group, autophagy of mitochondria increased, some mitochondria swelled and cristae of mitochondria decreased. In the EMO group, most of the mitochondria were in their normal state, and the mitochondrial cristae were visible. In contrast, the Nrf2 inhibitor group's mitochondria exhibited damage to the majority of them as well as the disappearance of the mitochondrial cristae. The mitochondrial damage of SAP + ML385 + EMO was partially recovered. The results revealed that SAP inhibited Nrf2 in rat lungs, which aggravated oxidative damage and mediated ferroptosis. Emodin may inhibit ferroptosis by activating the expression of Nrf2.

### Impact of EMO on Nrf2, HO-1, and GPX4 expression in the SAP-ALI rat model

To further ascertain the relationship between EMO and ferroptosis, we detected the genes related to the classical pathway of ferroptosis by PCR and WB. Rat lung tissue from the SAP group showed increased expressions of Nrf2 and HO-1 mRNA compared to the SO group but decreased expression of GPX4 mRNA. The Nrf2, HO-1, and GPX4 mRNA expressions in the EMO group were higher than those of the SAP group (Fig. 5A-C). At the translation level, the same trend also appeared (Fig. 5D-I). Simultaneously, the aforementioned genes and proteins were found to express differently in the lung tissue

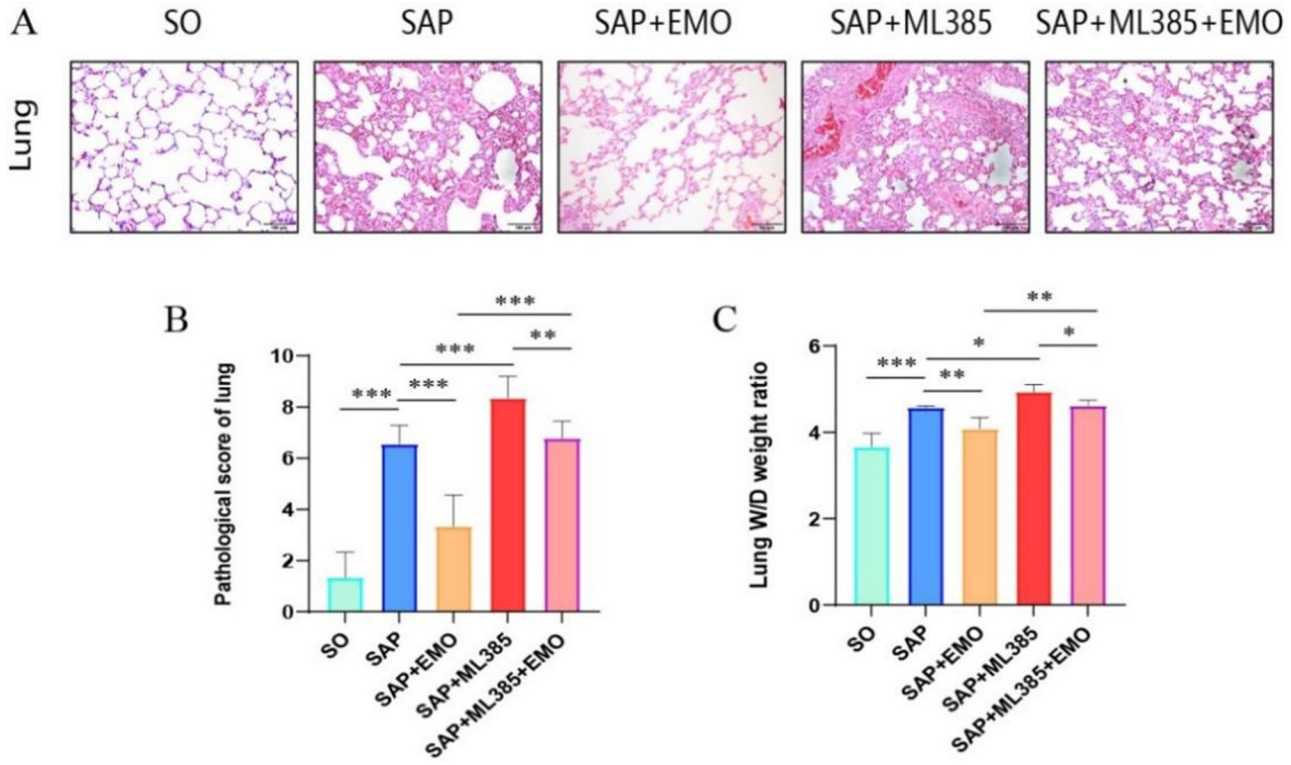


**Fig. 3** Inhibition of Nrf2 expression aggravated SAP-induced lung injury in rats, but EMO treatment reduced the degree of injury. (**A**) Lung tissue stained with hematoxylin-eosin (HE) (scale bar, 100 μm). (**B**) Quantitative analysis of lung tissue histopathological scores. (**C**) Lung W/D weight ratios. ***$p < 0.001$, **$p < 0.01$, *$p < 0.05$

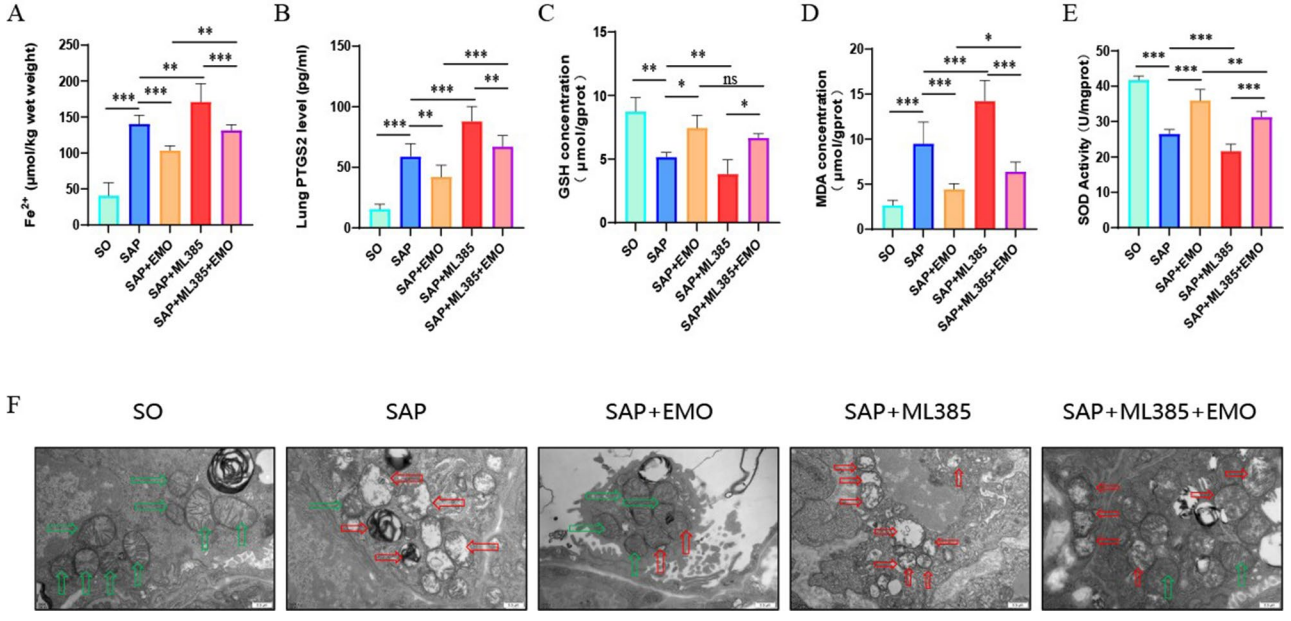


**Fig. 4** EMO may restrain oxidative damage and ferroptosis in SAP-ALI rats by activating Nrf2. (**A**) The level of $Fe^{2+}$ in the lung tissue. (**B**) PTGS2 level in the lung tissue. (**C**) GSH level in the lung tissue. (**D**) MDA level in the lung tissue. (**E**) SOD level in the lung tissue. (**F**) The mitochondrial morphology of rat alveolar epithelial cells was observed by transmission electron microscopy. The green arrow represents normal mitochondria; the red arrow represents aberrant mitochondria (scale bar, 0.5 μm). ***$p < 0.001$, **$p < 0.01$, *$p < 0.05$

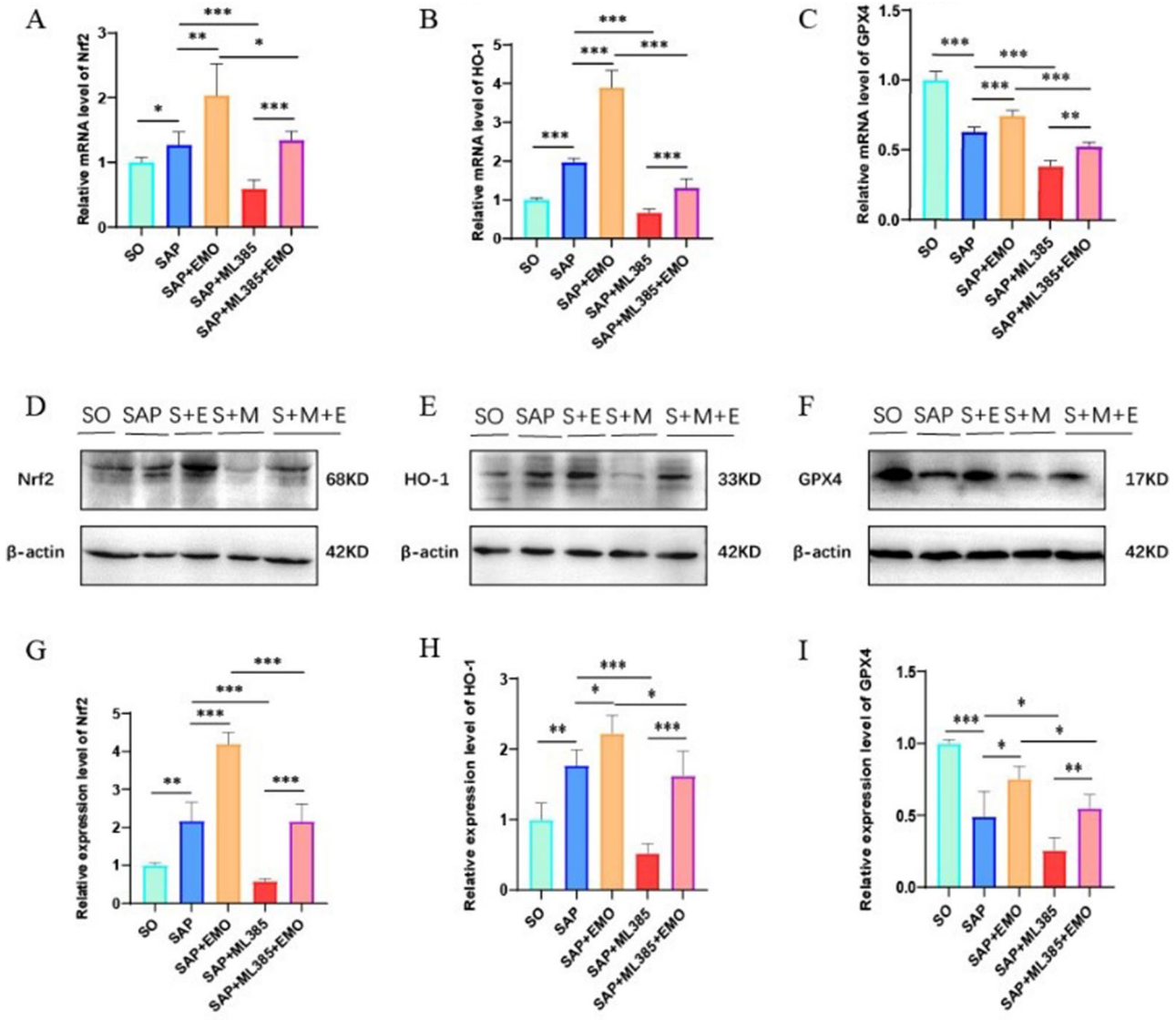


**Fig. 5** Levels of Nrf2, HO-1, and GPX4 in lung tissue of rats. (**A**-**C**) Nrf2, HO-1, and GPX4 mRNA levels in rat's lung tissue; (**D**-**I**) The loading control in rat lung tissue was β-actin, and the proteins Nrf2, HO-1, and GPX4 were measured. Full-length blots/gels are presented in Supplementary Fig. 1. ***$p < 0.001$, **$p < 0.01$, *$p < 0.05$

of rats in the SAP + ML385 group compared to the SAP group. The expression of Nrf2, HO-1, and GPX4 was found to be lower in the lung tissue of these rats. The expression of the SAP + ML385 + EMO group significantly increased compared to the SAP + ML385 group (Fig. 5A-I). The results demonstrated that in the rat model of SAP-induced lung injury, EMO activated Nrf2 and further activated the Nrf2/HO-1/GPX4 pathway.

### Molecular docking

EMO, Nrf2, HO-1, and GPX4 were respectively brought into molecular docking by AutoDockTools-1.5.7 software, and their binding energies were analyzed. The results showed that EMO had strong binding activity with Nrf2, HO-1, and GPX4. As Fig. 6 illustrates, the molecular docking visualization analysis of the above combinations was carried out using PyMOL software. It can be seen that EMO forms hydrogen bonds with lysine (Lys)-551 of Nrf2, phenylalanine (PHE)-169, glutamine (GLN)-145, and isoleucine (ILE)-172 of HO-1, and with methionine (MET)-26, histidine (HIS)-25, and asparagine (ASN)-28 of GPX4.

### Effects of EMO and Nrf2 inhibitor on the activity of A549 alveolar epithelial cells

The drug toxicity of emodin and the Nrf2 inhibitor (ML385) to the A549 alveolar epithelial cell line was determined by the CCK8 detection kit. The IC50 value is calculated by a 4-parameter regression of the logarithmic transformation curve using GraphPad Prism software.

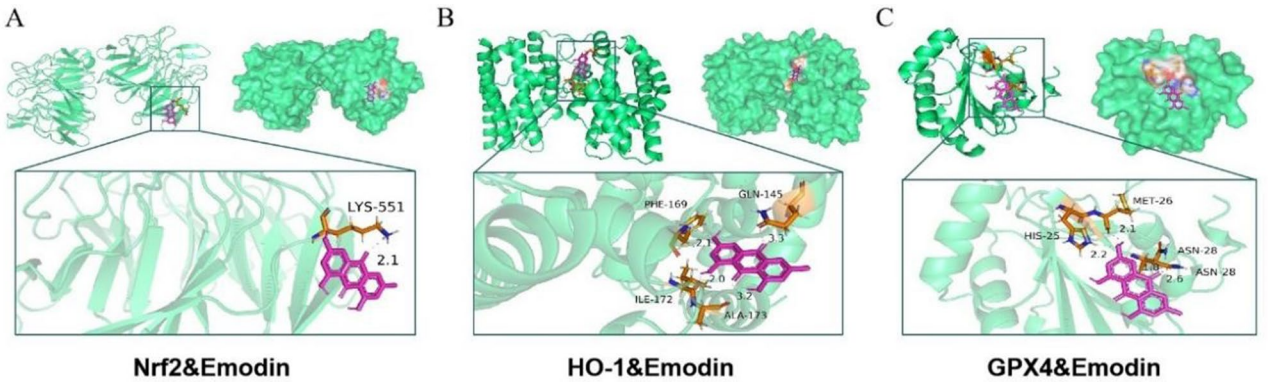


**Fig. 6** 3D images of molecular docking. (**A**) Molecular docking for EMO and Nrf2. (**B**) Molecular docking for EMO and HO-1. (**C**) Molecular docking for EMO and GPX4

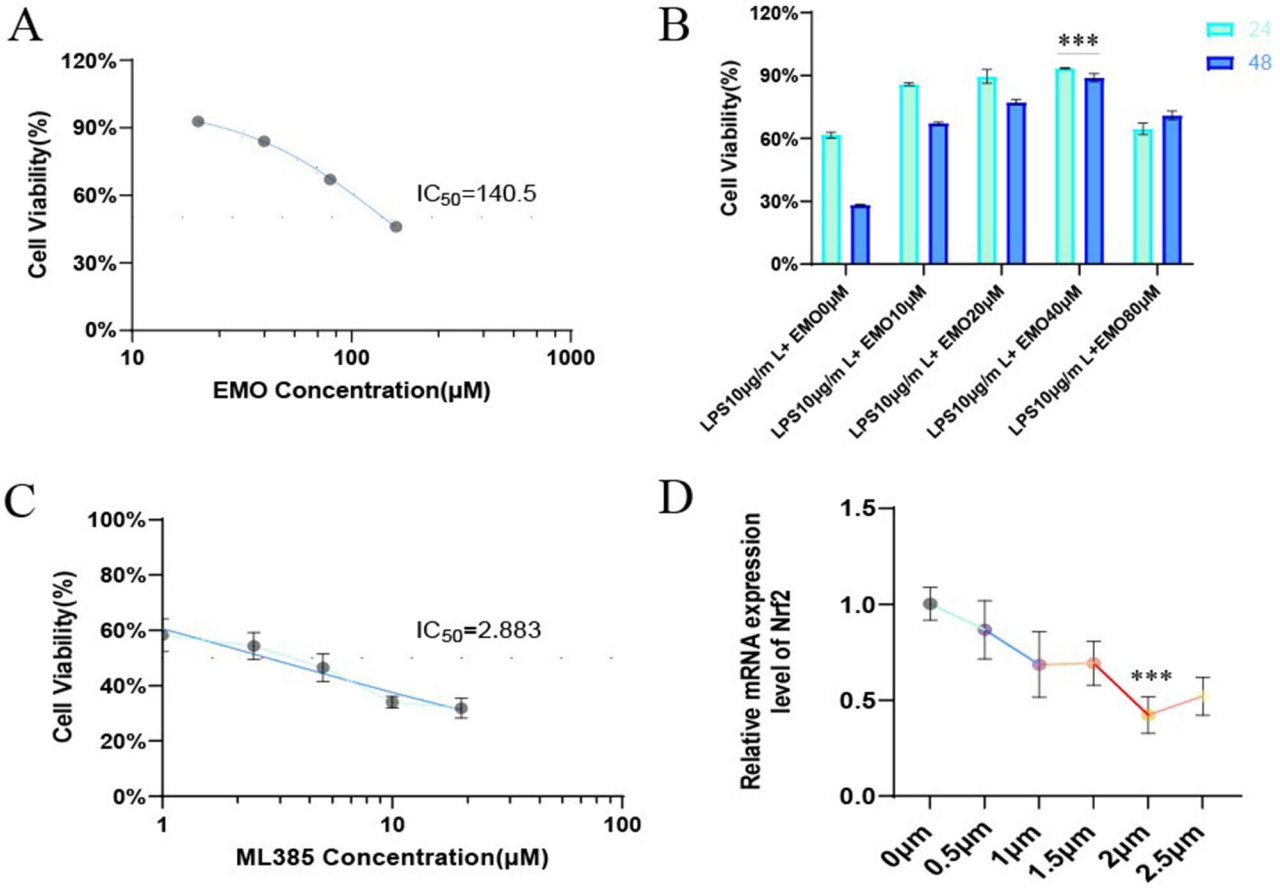


**Fig. 7** Analysis of drug concentration of EMO and ML385 in A549 alveolar epithelial cells. (**A**-**B**) Cellular activity was assessed in response to different EMO concentrations using the CCK8 technique. (**C**) CCK8 detection of drug toxicity of ML385 on A549 cells. (**D**) The amount of Nrf2 mRNA expression in cells stimulated by varying ML385 concentration gradients was detected by PCR. ***$p < 0.001$

The results showed that the half-maximal inhibitory concentrations (IC50) of EMO and ML385 on A549 cells were 140.5 μM (Fig. 7A) and 2.883 μM (Fig. 7C), respectively. Furthermore, the optimal drug concentration and intervention time of different concentration gradients of EMO were tested at 24 and 48 two time points. As shown in Fig. 7B, under the stimulation of LPS, the cell activity of the LPS 10 μg/mL + EMO 40 μM group was the highest in 24 h (Cells were exposed to 10 μg/mL LPS for 24 h [23, 24]). Finally, the optimal inhibitory concentration of ML385 on A549 cells was 2 μM by PCR (Fig. 7D). Therefore, 40 μM emodin and 2 μM ML385 were selected for the next experiment.

### Intervention with emodin reduced LPS-induced alveolar epithelial cell inflammatory damage

LPS stimulation resulted in a significant decrease in the activity of alveolar epithelial cells. After EMO intervention, the cell activity was improved, and the cell activity of inhibiting Nrf2 expression was lower than that of the LPS group, while EMO could reverse the further damage to cells caused by low Nrf2 expression (Fig. 8A). The inflammatory factors TNF-α, IL-1β, and IL-18 were found in significantly higher concentrations in the supernatant of alveolar epithelial cells in the model group compared to the CON group. The level of inflammatory factors above the cells in the inhibitor group increased uniformly and to different degrees compared to the model group. Furthermore, TNF-α, IL-1β, and IL-18 levels were lower in the EMO or LPS + ML385 + EMO groups than in the model or inhibitor groups, and the differences are statistically significant (Fig. 8B-D). These results indicated that EMO can alleviate the LPS-induced inflammatory reaction of alveolar epithelial cells by activating Nrf2.

### EMO inhibited oxidative damage of alveolar epithelial cells

Figure 9A-C shows that after LPS stimulates cells, the PTGS2 levels in the alveolar epithelial cells were considerably elevated, while the SOD and GSH levels were significantly decreased. The changes in the above indexes were more obvious in the inhibitor group, however, PTGS2 levels decreased and SOD or GSH consumption was reversed after EMO intervention. Subsequently, we further performed a fluorescence probe detection on the cell reactive oxygen species (ROS). The ROS fluorescence intensity in the LPS group is greater than in the CON

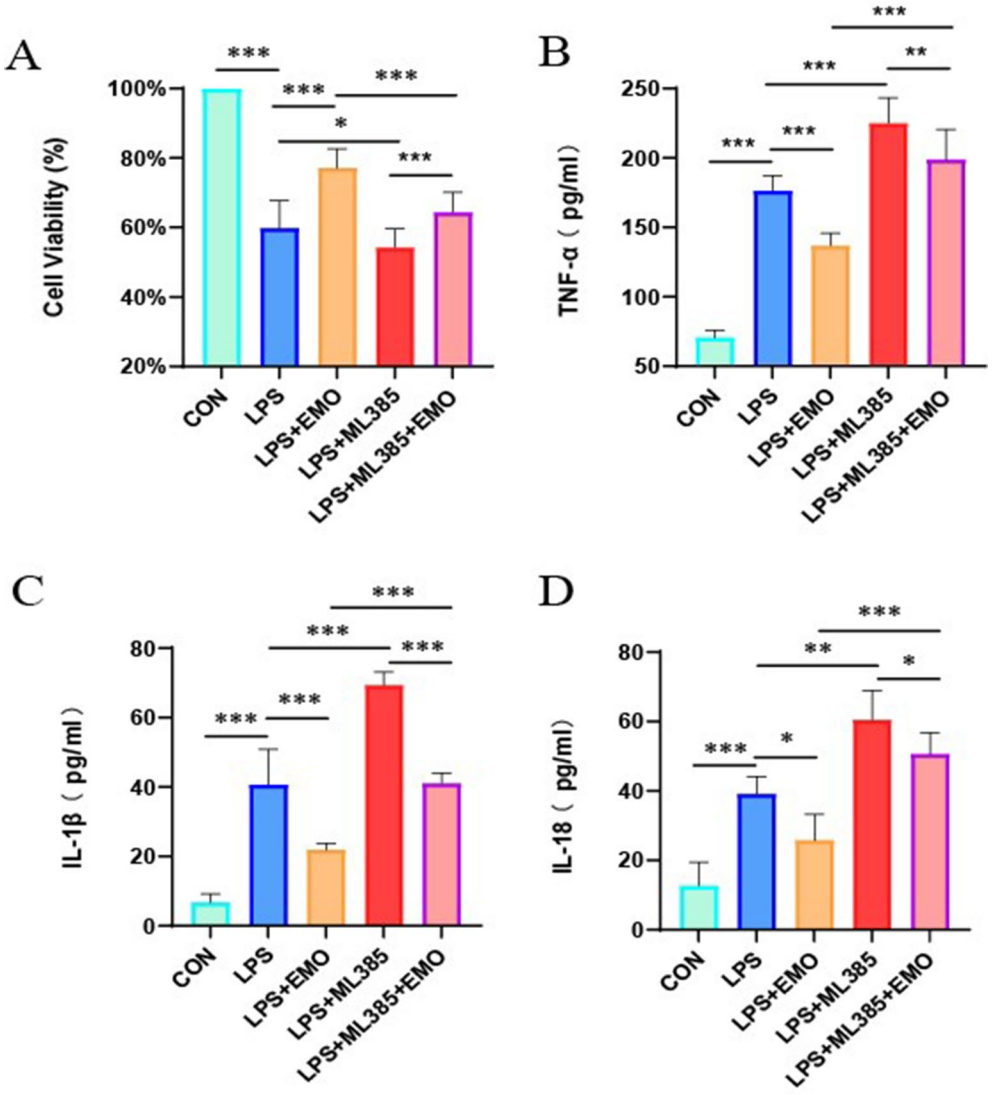


**Fig. 8** Emodin intervention relieved LPS-induced inflammatory reaction of alveolar epithelial cells. (**A**) The cell activity was assessed by the CCK8 kit. (**B**-**D**) The expression levels of TNF-α, IL-1β, and IL-18 in the cell supernatant were assessed using ELISA. ***$p < 0.001$, **$p < 0.01$, *$p < 0.05$

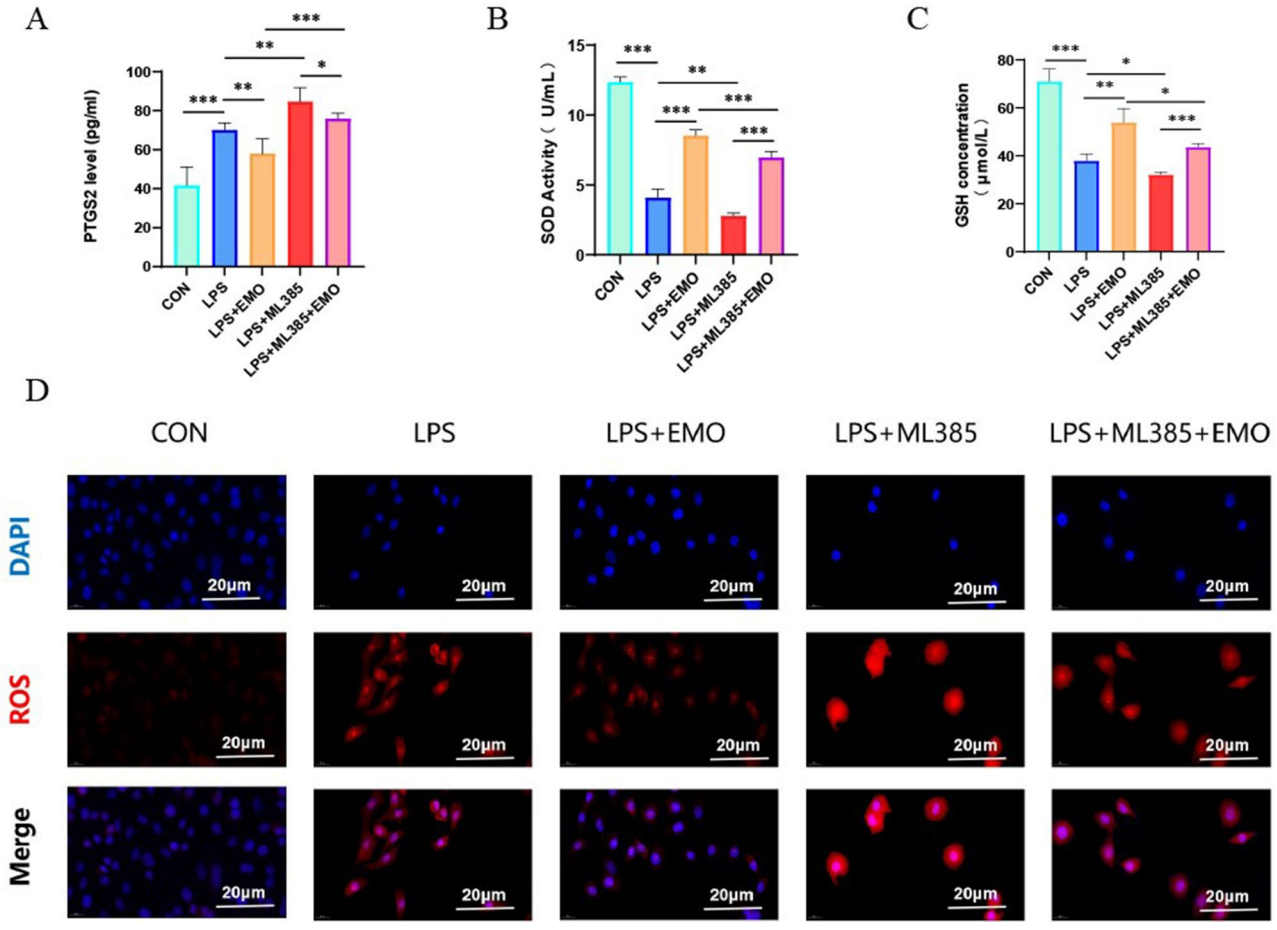


**Fig. 9** EMO inhibits oxidative damage of alveolar epithelial cells by activating Nrf2. (**A**-**C**) PTGS2, SOD, and GSH concentrations in cells. (**D**) The level of ROS in cells was detected by fluorescent probe (scale bar, 20 μm), the nucleus is blue and ROS is red. ***$p < 0.001$, **$p < 0.01$, *$p < 0.05$

group, as seen in Fig. 9D. However, the ROS fluorescence intensity in the cells weakened following the EMO intervention. Also, the ROS fluorescence intensity in the inhibitor group was noticeably higher than in the LPS or EMO groups, indicating that inhibiting cell Nrf2 significantly enhanced the effect of ROS on cells. According to the expected results, EMO intervention may inhibit ROS activity by activating Nrf2, so there was a decrease in ROS expression in the LPS + ML385 + EMO group. Consequently, EMO inhibits oxidative damage to alveolar epithelial cells by activating Nrf2.

### EMO intervention alveolar epithelial cells activated Nrf2/HO-1/GPX4 pathway in vitro

The main risk factor for ferroptosis in lung injury is an imbalance of the Nrf2/HO-1/GPX4 pathway [25]. Immunofluorescence staining, PCR, and WB results showed that EMO promoted Nrf2 nuclear translocation and upregulated the levels of HO-1 and GPX4, while ML385 reversed the impact of EMO on the Nrf2/HO-1/GPX4 pathway in vitro. (Fig. 10).

## Discussion

SAP is one of the most common digestive system diseases in clinics, and it is a pancreatitis disease, that is often accompanied by SIRS and MODS. The main clinical manifestations of SAP are abdominal pain, fever, nausea and vomiting, jaundice, hypotension or shock, gastrointestinal bleeding, skin and mucous membrane bleeding, etc. It is an acute abdomen with a sinister condition, many complications, and high mortality. ALI is the common complications of SAP and one of the main causes of death [26]. SAP-ALI is still a significant challenge for surgeons because of its high mortality. Therefore, more effective novel therapeutic agents are urgently needed. Our findings demonstrated that EMO effectively inhibited ferroptosis while promoting the Nrf2/HO-1/GPX4 signaling pathway, indicating that it may have application as an anti-ALI therapeutic agent.

*Rhei Radix Et Rhizoma* officinale is the first choice of traditional Chinese medicine for Tongligongxia. The primary active ingredient in *rhubarb*, emodin, has long been a focus of research because of its antiviral, antibacterial, and anti-inflammatory properties. Numerous

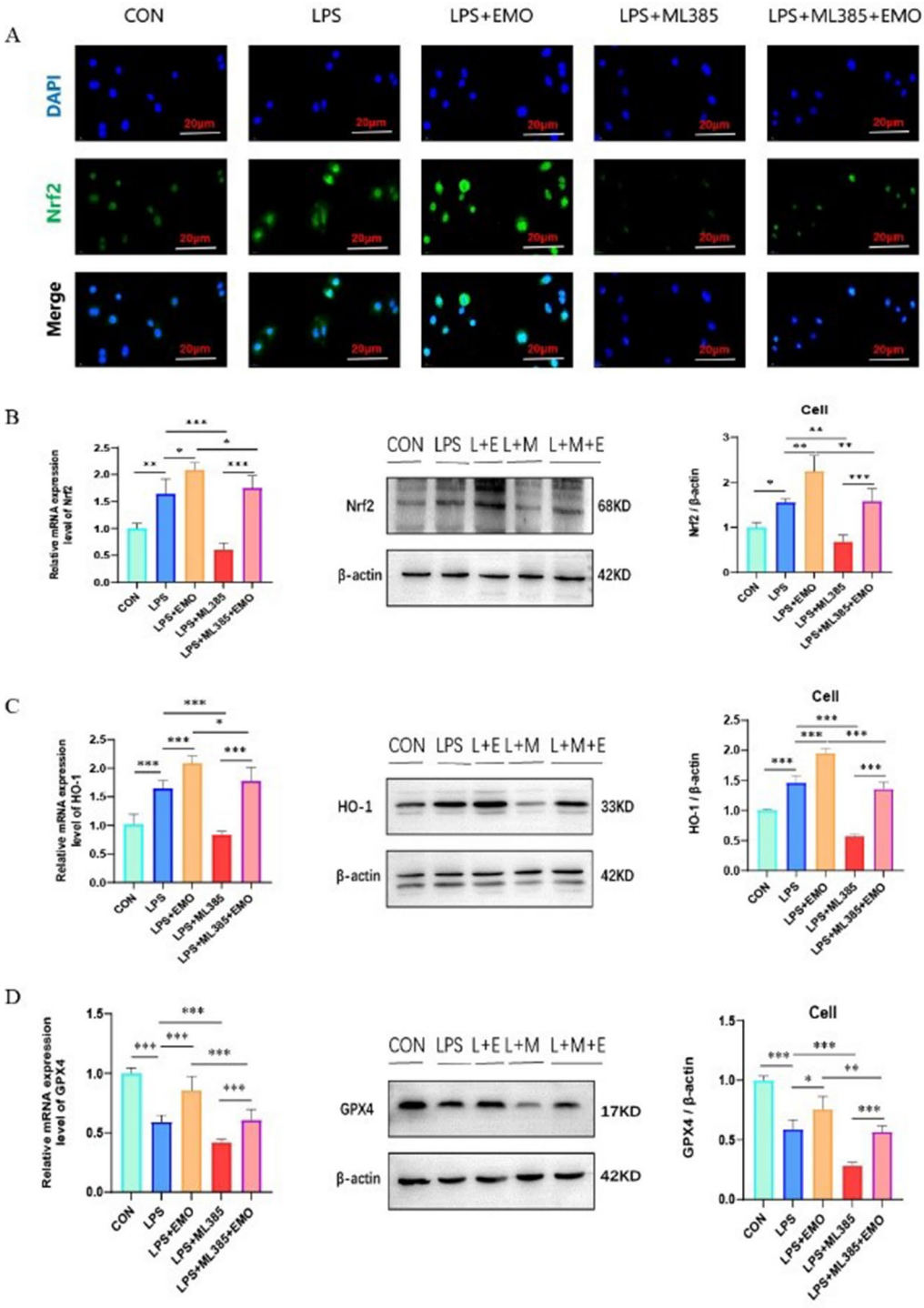


**Fig. 10** The Nrf2/HO-1/GPX4 pathway was activated in alveolar epithelial cells upon EMO intervention. (**A**) Immunofluorescence detection of Nrf2 in each group of cells, the nucleus is blue and Nrf2 is green (scale bar, 20 μm). (**B**-**D**) mRNA and protein expression levels of cells Nrf2, HO-1, and GPX4. Full-length blots/gels are presented in Supplementary Fig. 2. ***$p < 0.001$, **$p < 0.01$, *$p < 0.05$

studies have demonstrated the effectiveness of EMO in the treatment of SAP. The beneficial effect of combining baicalin and EMO in preventing pancreatic injury and inflammation in SAP rats was documented by Zhang et al. in 2005 [27]. Preclinical research conducted later on confirmed that EMO protects against a range of diseases caused by SAP, such as intestinal barrier dysfunction [28], liver injury [29], lung injury [30], and systemic inflammatory response [31, 32]. Our team has been devoted to researching the drug action of EMO on the

SAP-ALI disease model. Previous studies have proved that EMO can reduce the inflammatory injury and the severity of the disease by regulating the expression profiles of exosome-specific miRNA [18], inhibiting cold-induced RNA-binding protein (CIRP) [22], and inhibiting neutrophil protease activity [33]. Despite this, ferroptosis mediated by EMO in the pathogenesis of SAP-ALI is still unclear. The present investigation examined how EMO affected both LPS-induced alveolar epithelial cell damage and SAP-ALI. Accordingly, ferroptosis, oxidative damage, cell inflammation, and SAP-mediated pathological alterations were all considerably alleviated by EMO treatment.

Ferroptosis is a distinct type of cell death that differs from apoptosis, pyroptosis, and necrosis. Its primary symbol is unrestricted lipid peroxidation [34, 35]. Ferroptosis is widely perceived as promoting ALI development [36–38]. EMO has been suggested implicated in lipid peroxidation and oxidative stress [39, 40]. In this study, how ferroptosis affected SAP-ALI was investigated. As a result, in the SAP group, the expressions of $Fe^{2+}$, PTGS2, and MDA increased significantly, while the expressions of GSH, SOD and GPX4 decreased markedly. EMO treatment lowered $Fe^{2+}$, PTGS2, and MDA levels and partially recovered GSH, SOD, and GPX4 levels. Consequently, SAP-ALI developed ferroptosis, which was considerably reduced by EMO. Experiments have shown that ML385 is a potent Nrf2 inhibitor, and it can suppress Nrf2 expression both in vitro and in vivo [41, 42]. Except for promoting the consumption of GSH and SOD, ML385 treatment can raise the accumulation of $Fe^{2+}$, PTGS2, and MDA. Moreover, inhibition of Nrf2 aggravated mitochondrial damage of alveolar epithelial cells in SAP rats. Consequently, Nrf2 is a key indicator for ferroptosis, and the classical Nrf2 pathway mechanism of ferroptosis was further explored.

Nrf2 is the main antioxidant factor in cells, and it also regulates lipid peroxidation, ferredoxin, GSH synthesis and metabolism, and iron metabolism [43, 44]. In a physiologically normal state, Keap1 anchors Nrf2 in the cytoplasm. Keap1 is a substrate of the Cullin 3-dependent E3 ubiquitin ligase complex, which means that it can promote the ubiquitination of Nrf2 and quickly be broken down by the proteasome. Nevertheless, Nrf2 separates from Keap1 and then quickly undergoes nuclear translocation in response to ROS or electrophilic assault on cells. It first forms a heterodimer, and after that, it joins forces with an antioxidant response element (ARE) to trigger the antioxidant enzyme expression regulated by Nrf2 [45, 46]. Meanwhile, Nrf2 is also a leading transcription factor for HO-1, GPX, SOD, and GSH [47, 48]. HO-1 is expressed by macrophages, which can maintain heme homeostasis, prevent toxic decomposition caused by free heme, and release anti-inflammatory factors by catalyzing heme [49]. Induced HO-1 expression can lower ROS production and inflammatory cytokine secretion in inflammatory diseases like sepsis, which are crucial for tissue protection [50, 51]. As the only member of the selenoprotein family that can prevent ROS-mediated lipid peroxidation and hence prevent ferroptosis, GPX4 is a lipid repair enzyme that is usually employed as a critical molecular indicator of iron overload [52]. In this study, inhibition of Nrf2 in vitro and in vivo aggravated ALI induced by SAP in rats and alveolar epithelial cell injury mediated by LPS. In rat lungs, the particular pathological mechanism manifested by inhibiting Nrf2 dramatically reduced GSH and SOD levels, which in turn promoted loss of protective HO-1 and GPX4 levels, lipid peroxidation, and ferroptosis. Remarkably, EMO counteracted this effect, suggesting that by blocking SAP-mediated ferroptosis, it may be used as a therapy to prevent lung damage. The outcomes demonstrated that in both the LPS-induced injury of alveolar epithelial cells and the SAP-induced lung injury rat model, Nrf2 was activated by EMO, which also further activated the Nrf2/HO-1/GPX4 pathway. The suppressive effect of EMO on ferroptosis was significantly eliminated upon inhibition of the Nrf2/HO-1/GPX4 pathways. These findings provide new evidence for treating ALI with a new Nrf2 agonist EMO.

The present investigation, however, is restricted to in vitro research and animal models lacking clinical data. Further extensive and comprehensive research is needed to explore the connection between ferroptosis and EMO in the SAP-ALI disease model and establish a theoretical framework for future clinical investigations.

## Conclusions

In the lung tissue of SAP rats and alveolar epithelial cells, ferrous ion accumulation, lipid peroxidation, and ROS accumulation are indicative of ferroptosis and oxidative damage. EMO has a significant antioxidant effect, which may be through inhibiting $Fe^{2+}$ and PTGS2, reducing the level of MDA, reducing the accumulation of ROS, and alleviating oxidative stress injury, thus improving lung function and cell activity, and slowing down the occurrence and development of SAP-ALI by modulating the Nrf2/HO-1/GPX4 axis. The goal of the follow-up research is to confirm the findings by delving deeper into the pathophysiology of SAP-ALI through clinical experiments and offering promising new avenues for clinical prevention and treatment of the illness.

### Abbreviations

| | |
|---|---|
| SAP | Severe acute pancreatitis |
| ALI | Acute lung injury |
| EMO | Emodin |
| SO | Sham operation group |
| STC | Sodium taurocholate |
| Nrf2 | Nuclear factor erythroid 2-related factor 2 |
| LPS | Lipopolysaccharide |
| ELISA | Enzyme-linked immunosorbent assays |

| | |
|---|---|
| PCR | Real-time polymerase chain reaction |
| WB | Western blot |
| HO-1 | Heme Oxygenase-1 |
| GPX4 | Glutathione peroxidase 4 |
| GSH | Glutathione |
| MDA | Malondialdehyde |
| SOD | Superoxide dismutase |
| ROS | Reactive oxygen species |
| ARE | Antioxidant response element |
| BNCC | The BeNa Culture Collection |
| CON | control |
| W/D | Wet/Dry |
| A | Absorbance |
| ANOVA | one-way analysis of variance |
| PTGS2 | Prostaglandin-endoperoxide synthase 2 |
| TEM | Transmission electron microscope |
| Lys | Lysine |
| PHE | Phenylalanine |
| GLN | Glutamine |
| ILE | Isoleucine |
| MET | Methionine |
| HIS | Histidine |
| ASN | Asparagine |
| CIRP | Cold-induced RNA-binding protein |

## Supplementary Information

The online version contains supplementary material available at https://doi.org/10.1186/s12876-025-03660-1 .

Supplementary Material 1

Supplementary Material 2

**Acknowledgements**
Not applicable.

**Author contributions**
SG and WHY contributed to the study concept and design, execution of experiments, interpretation of data, acquisition of data, statistical analysis, and writing of the manuscript. LHJ and ZXT optimized, performed, and analyzed the western blot experiments. LBW and DXC assisted in animal experiment modeling and material collection. GP and LYL contributed to the study concept and provided critical revision of the manuscript for important intellectual content. CHL contributed to the study concept, design, supervision, and provided critical revision of the manuscript for important intellectual content. All authors read and approved the final manuscript.

**Funding**
This study was supported by the National Natural Science Foundation of China (No. 82274311 and 82074158) and the Dalian Medical Science Research Program Project (No. 2211024).

**Data availability**
The crystal structures of Nrf2, HO-1, and GPX4 were downloaded from the PDB database (https://www.rcsb.org), and the 3D structure of emodin was obtained from the PubChem database (https://pubchem.ncbi.nlm.nih.gov). The datasets used and/or analysed during the current study are available from the corresponding author on reasonable request.

## Declarations

**Ethics approval and consent to participate**
The animal study protocol was approved by the Dalian Medical University's Laboratory Animal Ethics Committee (permission no. AEE23067). As mandated by China Animal Protection and Use Committee regulations, every effort was made to guarantee the comfort and welfare of the animals throughout the studies.

**Consent for publication**
Not applicable.

**Competing interests**
The authors declare no competing interests.

**Author details**
[1]Department of General Surgery, Pancreatic-Biliary Center, The First Affiliated Hospital of Dalian Medical University, No. 222 Zhongshan Road, Dalian, Liaoning Province 116011, People's Republic of China
[2]Institute (College) of Integrative Medicine, Dalian Medical University, Dalian Liaoning 116011, People's Republic of China
[3]Laboratory of Integrative Medicine, The First Affiliated Hospital of Dalian Medical University, Dalian Liaoning 116011, People's Republic of China
[4]The First Affiliated Hospital of Dalian Medical University, Dalian Liaoning 116011, People's Republic of China
[5]Dalian Women and Children's Medical Center (Group), Dalian Medical University, Dalian Liaoning 116011, People's Republic of China
[6]Department of Gastroenterology, The First Affiliated Hospital of Dalian Medical University, Dalian Liaoning 116011, People's Republic of China

Received: 8 November 2024 / Accepted: 30 January 2025
Published online: 05 February 2025

**References**

1. Barreto SG, Habtezion A, Gukovskaya A, et al. Critical thresholds: key to unlocking the door to the prevention and specific treatments for acute pancreatitis. Gut. 2021;70(1):194–203.
2. Beyer G, Hoffmeister A, Lorenz P, Lynen P, Lerch MM, Mayerle J. Clinical practice Guideline—Acute and Chronic Pancreatitis. Dtsch Arztebl Int. 2022;119(29–30):495–501.
3. Cao Y, Li F, Sun Z, et al. Regulation of Microtubule Stability in Pulmonary Microvascular endothelial cells in rats with severe Acute Pancreatitis: Qingyi Decoction is a potential CDK5 inhibitor. J Inflamm Res. 2024;17:2513–30.
4. El-Horany HE, Atef MM, Abdel Ghafar MT et al. Empagliflozin ameliorates Bleomycin-Induced Pulmonary fibrosis in rats by modulating Sesn2/AMPK/Nrf2 signaling and targeting ferroptosis and autophagy. Int J Mol Sci. 2023. 24(11).
5. Feng L, Wang C, Zhang C, et al. p38 MAPK inhibitor SB202190 suppresses ferroptosis in the glutamate-induced retinal excitotoxicity glaucoma model. Neural Regen Res. 2024;19(10):2299–309.
6. Wang Z, Zhou W, Zhang Z, Zhang L, Li M. Metformin alleviates spinal cord injury by inhibiting nerve cell ferroptosis through upregulation of heme oxygenase-1 expression. Neural Regen Res. 2024;19(9):2041–9.
7. Ma D, Li C, Jiang P, Jiang Y, Wang J, Zhang D. Inhibition of ferroptosis attenuates acute kidney Injury in rats with severe Acute Pancreatitis. Dig Dis Sci. 2021;66(2):483–92.
8. Li Y, Cao Y, Xiao J, et al. Inhibitor of apoptosis-stimulating protein of p53 inhibits ferroptosis and alleviates intestinal ischemia/reperfusion-induced acute lung injury. Cell Death Differ. 2020;27(9):2635–50.
9. Zhang H, Wu D, Wang Y, et al. METTL3-mediated N6-methyladenosine exacerbates ferroptosis via m6A-IGF2BP2-dependent mitochondrial metabolic reprogramming in sepsis-induced acute lung injury. Clin Transl Med. 2023;13(9):e1389.
10. Li Z, Yu Y, Bu Y, et al. QiShenYiQi pills preserve endothelial barrier integrity to mitigate sepsis-induced acute lung injury by inhibiting ferroptosis. J Ethnopharmacol. 2024;322:117610.
11. Htut NW, Onkoksoong T, Saelim M, Kueanjinda P, Sampattavanich S, Panich U. Live-cell imaging unveils stimulus-specific dynamics of Nrf2 activation in UV-exposed melanoma cells: implications for antioxidant compound screening. Free Radic Biol Med. 2024;211:1–11.
12. Wei D, Qu C, Zhao N, et al. The significance of precisely regulating heme oxygenase-1 expression: another avenue for treating age-related ocular disease. Ageing Res Rev. 2024;97:102308.
13. Deng L, Di Y, Chen C, et al. Depletion of the N(6)-Methyladenosine (m6A) reader protein IGF2BP3 induces ferroptosis in glioma by modulating the expression of GPX4. Cell Death Dis. 2024;15(3):181.
14. Stompor-Gorący M. The Health benefits of Emodin, a natural anthraquinone derived from Rhubarb-A Summary Update. Int J Mol Sci. 2021;22(17):9522.
15. Ye Y, Zhong W, Luo R, et al. Thermosensitive hydrogel with emodin-loaded triple-targeted nanoparticles for a rectal drug delivery system in the treatment of chronic non-bacterial prostatitis. J Nanobiotechnol. 2024;22(1):33.

16. Hu Q, Yao J, Wu X, et al. Emodin attenuates severe acute pancreatitis-associated acute lung injury by suppressing pancreatic exosome-mediated alveolar macrophage activation. Acta Pharm Sin B. 2022;12(10):3986–4003.
17. Wu X, Yao J, Hu Q, et al. Emodin ameliorates Acute Pancreatitis-Associated Lung Injury through inhibiting the alveolar macrophages pyroptosis. Front Pharmacol. 2022;13:873053.
18. Yang Q, Luo Y, Ge P, et al. Emodin ameliorates severe Acute Pancreatitis-Associated Acute Lung Injury in rats by modulating exosome-specific miRNA expression profiles. Int J Nanomed. 2023;18:6743–61.
19. Cui H, Li S, Xu C, Zhang J, Sun Z, Chen H. Emodin alleviates severe acute pancreatitis-associated acute lung injury by decreasing pre-B-cell colony-enhancing factor expression and promoting polymorphonuclear neutrophil apoptosis. Mol Med Rep. 2017;16(4):5121–8.
20. Rongione AJ, Kusske AM, Kwan K, Ashley SW, Reber HA, McFadden DW. Interleukin 10 reduces the severity of acute pancreatitis in rats. Gastroenterology. 1997;112(3):960–7.
21. Osman MO, Kristensen JU, Jacobsen NO, et al. A monoclonal anti-interleukin 8 antibody (WS-4) inhibits cytokine response and acute lung injury in experimental severe acute necrotising pancreatitis in rabbits. Gut. 1998;43(2):232–9.
22. Xu Q, Wang M, Guo H, et al. Emodin alleviates severe Acute Pancreatitis-Associated Acute Lung Injury by inhibiting the Cold-Inducible RNA-Binding protein (CIRP)-Mediated activation of the NLRP3/IL-1β/CXCL1 signaling. Front Pharmacol. 2021;12:655372.
23. Xiong X, Dou J, Shi J, et al. RAGE inhibition alleviates lipopolysaccharides-induced lung injury via directly suppressing autophagic apoptosis of type II alveolar epithelial cells. Respir Res. 2023;24(1):24.
24. Zeng H, Zhou Y, Liu Z, Liu W. MiR-21-5p modulates LPS-induced acute injury in alveolar epithelial cells by targeting SLC16A10. Sci Rep. 2024;14(1):11160.
25. Lou L, Wang M, He J, et al. Urolithin A (UA) attenuates ferroptosis in LPS-induced acute lung injury in mice by upregulating Keap1-Nrf2/HO-1 signaling pathway. Front Pharmacol. 2023;14:1067402.
26. Landahl P, Ansari D, Andersson R. Severe Acute Pancreatitis: gut barrier failure, systemic inflammatory response, Acute Lung Injury, and the role of the Mesenteric Lymph. Surg Infect (Larchmt). 2015;16(6):651–6.
27. Zhang XP, Li ZF, Liu XG, et al. Effects of emodin and baicalein on rats with severe acute pancreatitis. World J Gastroenterol. 2005;11(14):2095–100.
28. Ning JW, Zhang Y, Yu MS, et al. Emodin alleviates intestinal mucosal injury in rats with severe acute pancreatitis via the caspase-1 inhibition. Hepatobiliary Pancreat Dis Int. 2017;16(4):431–6.
29. Wang G, Sun B, Gao Y, Meng QH, Jiang HC. The effect of emodin-assisted early enteral nutrition on severe acute pancreatitis and secondary hepatic injury. Mediators Inflamm. 2007. 2007: 29638.
30. Xia XM, Wang FY, Wang ZK, Wan HJ, Xu WA, Lu H. Emodin enhances alveolar epithelial barrier function in rats with experimental acute pancreatitis. World J Gastroenterol. 2010;16(24):2994–3001.
31. Ni Q, Sun K, Chen G, Shang D. In vitro effects of emodin on peritoneal macrophages that express membrane-bound CD14 protein in a rat model of severe acute pancreatitis/systemic inflammatory response syndrome. Mol Med Rep. 2014;9(1):355–9.
32. Wang GJ, Wang Y, Teng YS et al. Protective Effects of Emodin-Induced Neutrophil Apoptosis via the Ca (2+)-Caspase 12 Pathway against SIRS in Rats with Severe Acute Pancreatitis. Biomed Res Int. 2016. 2016: 1736024.
33. Xu C, Zhang J, Liu J, et al. Proteomic analysis reveals the protective effects of emodin on severe acute pancreatitis induced lung injury by inhibiting neutrophil proteases activity. J Proteom. 2020;220:103760.
34. Chen X, Tsvetkov AS, Shen HM et al. International consensus guidelines for the definition, detection, and interpretation of autophagy-dependent ferroptosis. Autophagy. 2024: 1–34.
35. Zhang R, Kang R, Tang D. Gut Microbiome mediates Ferroptosis Resistance for Colorectal Cancer Development. Cancer Res. 2024;84(6):796–7.
36. Wang X, Wei T, Luo J et al. Iron Overload-Dependent Ferroptosis Aggravates LPS-Induced Acute Lung Injury by Impairing Mitochondrial Function. Inflammation. 2024.
37. Xiong L, Liu Y, Wang Y, et al. The protective effect of Lonicera japonica Thunb. Against lipopolysaccharide-induced acute lung injury in mice: modulation of inflammation, oxidative stress, and ferroptosis. J Ethnopharmacol. 2024;331:118333.
38. Xu Z, Li J, Zhou K, et al. Exocarpium Citri Grandis ameliorates LPS-induced acute lung injury by suppressing inflammation, NLRP3 inflammasome, and ferroptosis. J Ethnopharmacol. 2024;329:118162.
39. Chen Q, Lai C, Chen F, et al. Emodin protects SH-SY5Y cells against Zinc-Induced synaptic impairment and oxidative stress through the ERK1/2 pathway. Front Pharmacol. 2022;13:821521.
40. Shen Z, Zhao L, Yoo SA et al. Emodin induces ferroptosis in colorectal cancer through NCOA4-mediated ferritinophagy and NF-κb pathway inactivation. Apoptosis. 2024.
41. Kong L, Liu Y, Li J, et al. Ginsenoside Rg1 alleviates chronic inflammation-induced neuronal ferroptosis and cognitive impairments via regulation of AIM2 - Nrf2 signaling pathway. J Ethnopharmacol. 2024;330:118205.
42. Xu S, Chen Y, Miao J, et al. Esculin inhibits hepatic stellate cell activation and CCl(4)-induced liver fibrosis by activating the Nrf2/GPX4 signaling pathway. Phytomedicine. 2024;128:155465.
43. Chen N, Hu M, Jiang T, Xiao P, Duan JA. Insights into the molecular mechanisms, structure-activity relationships and application prospects of polysaccharides by regulating Nrf2-mediated antioxidant response. Carbohydr Polym. 2024;333:122003.
44. Lan J, Liu L, Zhao W, et al. Unlocking the anticancer activity of gambogic acid: a shift towards ferroptosis via a GSH/Trx dual antioxidant system. Free Radic Biol Med. 2024;218:26–40.
45. Ho CY, Cheng YT, Chau CF, Yen GC. Effect of diallyl sulfide on in vitro and in vivo Nrf2-mediated pulmonic antioxidant enzyme expression via activation ERK/p38 signaling pathway. J Agric Food Chem. 2012;60(1):100–7.
46. Heiss EH, Schachner D, Zimmermann K, Dirsch VM. Glucose availability is a decisive factor for Nrf2-mediated gene expression. Redox Biol. 2013;1(1):359–65.
47. Dinkova-Kostova AT, Kostov RV, Kazantsev AG. The role of Nrf2 signaling in counteracting neurodegenerative diseases. FEBS J. 2018;285(19):3576–90.
48. Wang H, Han J, Dmitrii G, Zhang XA. Potential targets of Natural products for improving Cardiac Ischemic Injury: the role of Nrf2 Signaling Transduction. Molecules. 2024. 29(9).
49. Haodang L, Lianmei Q, Ranhui L, et al. HO-1 mediates the anti-inflammatory actions of sulforaphane in monocytes stimulated with a mycoplasmal lipopeptide. Chem Biol Interact. 2019;306:10–8.
50. Guo J, Miao Y, Nie F, et al. Zn-Shik-PEG nanoparticles alleviate inflammation and multi-organ damage in sepsis. J Nanobiotechnol. 2023;21(1):448.
51. Chen J, Zhou L, Li X, et al. Protective effect of zerumbone on sepsis-induced acute lung injury through anti-inflammatory and antioxidative activity via NF-κB pathway inhibition and HO-1 activation. Naunyn Schmiedebergs Arch Pharmacol. 2024;397(4):2241–55.
52. Liu Y, Wan Y, Jiang Y, Zhang L, Cheng W. GPX4: the hub of lipid oxidation, ferroptosis, disease and treatment. Biochim Biophys Acta Rev Cancer. 2023;1878(3):188890.

## Publisher's note